Weather and Climate Extremes 37 (2022) 100479

Contents lists available at ScienceDirect

Weather and Climate Extremes

journal homepage: www.elsevier.com/locate/wace

How do groundwater dynamics influence heatwaves in southeast Australia?

Mengyuan Mu [a,*], Andrew J. Pitman [a], Martin G. De Kauwe [b], Anna M. Ukkola [a], Jun Ge [c]

[a] ARC Centre of Excellence for Climate Extremes and Climate Change Research Centre, University of New South Wales, Sydney, NSW, Australia
[b] School of Biological Sciences, University of Bristol, Bristol, UK
[c] Institute for Climate and Global Change Research, School of Atmospheric Sciences, Nanjing University, Nanjing, 210023, China

A B S T R A C T

Groundwater plays an integral role in land-atmosphere interactions by connecting the sub-surface storage of water to transpiration via interactions with the root zone. The role of groundwater in moderating heatwave intensity has rarely been examined in coupled climate simulations, as many models overlook this key component of the water cycle. We use a coupled land-atmosphere model with an explicit representation of groundwater dynamics to analyze three major heatwave events in southeast Australia. Groundwater moistens and cools the land surface, with impacts extending to the top of the atmospheric boundary layer during heatwaves. Associated with the cooling, an increase of net radiation and a reduction in the atmospheric boundary layer height occurred, primarily over areas with a shallow water table depth and woody vegetation. The maximum air temperatures were reduced by up to 3 °C at the surface and up to 1 °C through the atmospheric boundary layer. Our results point to an important influence of groundwater on heatwave intensity, implying the necessity of considering groundwater dynamics in climate models in the future heatwave predications.

1. Introduction

Heatwaves that occur in Australian summers can severely disrupt ecosystems (Bergstrom et al., 2021; Ruthrof et al., 2018), cause major impacts to human societies (Borchers Arriagada et al., 2020; Zander et al., 2015), and lead to human mortality (Coates et al., 2014). A trend of increasing heatwave frequency and intensity in the southeast of Australia over the last few decades (Perkins-Kirkpatrick and Gibson, 2017; Perkins-Kirkpatrick and Lewis, 2020) has been coincident with an increase in the frequency of extremely high temperatures (Jyoteeshkumar reddy et al., 2021). For example, there were 33 days that the national daily average maximum temperatures exceeded 39 °C in 2019, more than the total observed from 1960 to 2018 (24 days; Bureau of Meteorology, 2020). Climate projections suggest this trend will continue and that Australia needs to be prepared for more intense, frequent and longer duration heatwaves (Lewis et al., 2017; Trancoso et al., 2020). Heatwaves in Australia are commonly associated with a stationary high pressure system which leads to an advection of hot and dry air from continental interior to the southeast coast (Pezza et al., 2012; Purich et al., 2014). While the generation of a heatwave is associated with the synoptic situation (Parker et al., 2014; Pezza et al., 2012), and changes in the frequency and duration of heatwaves are largely explained by changes in synoptic systems and associated circulation patterns (Kornhuber et al., 2020; Wehrli et al., 2019), the intensity of a heatwave can be influenced by land surface processes (Herold et al., 2016; Hirsch et al., 2014a, 2014b; Merrifield et al., 2019; Wehrli et al., 2019).

The key influence of the land surface on heatwave intensity is related to the partitioning of available energy between the sensible (Q_h) and latent heat (Q_e) fluxes. A wet surface can cool and moisten the lower atmosphere via evaporation, slowing the accumulation of heat in the atmospheric boundary layer (ABL) and potentially suppressing heatwave intensity. In contrast, a dry soil will tend to lead to higher Q_h which heats the ABL, and can intensify a heatwave. The increase of air temperature also leads to an increase in the amount of water vapour that can be held in the atmosphere, increasing the driving force for evaporation, which in turn accelerates soil desiccation (Miralles et al., 2014, 2019). Therefore, for specific heatwave events, the ability of vegetated and non-vegetated surfaces to access water for evaporative cooling is important, which depends on the topsoil water availability (Kala et al., 2015a, 2015b), the root zone moisture (potentially influenced by the shallow groundwater; Barlage et al., 2021; Martinez et al., 2016; Miguez-Macho et al., 2007; Mu et al., 2021b), the nature of the vegetation (e.g. root characteristics; Evaristo and McDonnell, 2017), and hydraulic redistribution (Luo et al., 2016).

The existence of groundwater is important for Australian ecosystems. Approximately 34% of land areas have the potential for groundwater-dependent ecosystems and 5% of these areas are heavily reliant on groundwater (Doody et al., 2017). Previous uncoupled simulations using the Community Atmosphere Biosphere Land Exchange (CABLE) land surface model (LSM) has shown the presence of shallow groundwater

* Corresponding author.
E-mail address: mengyuan.mu@unsw.edu.au (M. Mu).

https://doi.org/10.1016/j.wace.2022.100479
Received 28 January 2022; Received in revised form 24 May 2022; Accepted 29 June 2022
Available online 9 July 2022

influenced the surface energy balance and reduced forest canopy temperature by up to 0.76 °C on average during heatwaves over southeastern (S.E.) Australia (Mu et al., 2021b). However, these uncoupled simulations cannot show whether the land surface fluxes are large enough, or sustained for long enough, to affect the atmosphere and whether the land-atmosphere positive feedbacks act to increase the heatwave intensity. While there is evidence that perturbing soil moisture or using realistic initial soil moisture can influence heatwaves in S.E. Australia (e.g. Kala et al., 2015a, 2015b; Hirsch et al., 2014a, 2014b) this evidence focusses on perturbing soil moisture directly, not examining whether capturing the explicit dynamics of groundwater behaviour can influence Australian heatwaves.

Here, we examine the role of groundwater on heatwaves over S.E. Australia by focusing on the three significant events that occurred in 2009, 2013 and 2019. We use a coupled modelling system to answer three questions:

1. How does the existence of groundwater influence the water and energy balance during heatwaves?
2. To what degree does groundwater influence the atmosphere during heatwaves?
3. What are the key factors controlling the impact of groundwater on heatwaves?

Most climate models still do not account for groundwater dynamics and therefore the role played by the presence or absence of groundwater on heat extremes has not been widely examined. While the study by Keune et al. (2016) focused on the 2003 European heatwave, they reinitialized their atmospheric model every day which precludes representation of heat accumulation in the boundary layer over several days. The other coupled studies (e.g. Barlage et al., 2021; Forrester and Maxwell, 2020) mostly focused on the impact of groundwater on the seasonal or longer term climate rather than extreme events (Furusho-Percot et al., 2022). Therefore, we seek to identify whether the lack of groundwater processes in most climate models is potentially significant and whether the impact is localized or widespread in heatwave events.

2. Methods

2.1. Heatwave case studies

We investigated three severe heatwaves that occurred in 2009, 2013 and 2019 in S.E. Australia (Table 1). The first example heatwave occurred in late January and early February 2009 and affected S.E. Australia, when this region was in the last year of Australian Millennia Drought and land was relatively dry. The active monsoon trough and a strong tropical low near the northwest coast of the continent combined with a slow-moving high pressure system over the Tasman Sea that led a hot northerly air flow over southern Australia (Climate Centre, 2009). This event set new high temperature (e.g. 48.8 °C in Victoria and 42.2 °C in Tasmania) and duration records in parts of southern New South Wales and South Australia, Victoria, and northeastern Tasmania (Climate Centre, 2009). It affected more than one million people, caused 420 casualties, and led to A$800 million of financial losses (Kiem et al., 2010). The subsequent catastrophic Black Saturday bushfires (Engel et al., 2013) killed 173 people and caused more than $4 billion in economic losses (Teague et al., 2010).

Table 1
Details of the three heatwaves examined in this paper.

Heatwave periods	Heatwave peak days	Simulation periods
28 Jan–8 Feb 2009	28–31 Jan and 5–8 Feb 2009	18/19/20/21/22 Jan–13 Feb 2009
4–18 Jan 2013	4–8, 12–13 and 17–18 Jan 2013	25/26/27/28/29 Dec 2012–23 Jan 2013
14–26 Jan 2019	14–18 and 22–26 Jan 2019	4/5/6/7/8–31 Jan 2019

The second example, which influenced most of Australia in late December 2012 and the first two weeks of January 2013 followed one of the warmest springs on record (Bureau of Meteorology, 2013). This heatwave started from December 25, 2012 in the southwest of Western Australia. As the high pressure system over Great Australia Bight moved eastward, northerly winds advected intense heat into S.E. Australia such that 4th January was one of the hottest days recorded for southern Tasmania and coastal Victoria and South Australia. On 11th January, a second eastward-moving high pressure system led to further advection of very hot air and caused the second phase of extreme heat over S.E. Australia on 12–13th January. The north-westerly winds led the last heatwave over the study region on 17–18th January (Bureau of Meteorology, 2013). This heatwave broke the high temperature records in every state and territory, rendering January 2013 one of the hottest months on record (Bureau of Meteorology, 2013). The national mean maximum temperature of 40.3 °C on January 7, 2013 exceeded the previous record of 39.8 °C on January 1, 1973.

The final heatwave began in early December 2018, and extended through to January 2019 which was in the last year of the 2017–2019 drought. A series of intense heatwaves occurred across Australia leading to nationally averaged mean maxima above 40 °C from the 12th to the 16th January and rendered the 2018/2019 summer the hottest experienced for New South Wales, Victoria, Western Australia and the Northern Territory (Bureau of Meteorology, 2019). There were three distinct heatwave peaks, late December and early January, mid-January and late January, which persisted over most of the continent for several weeks. Due to the lack of thunderstorms and monsoonal activity, sequential sunny days provided ideal conditions for heat accumulation. As a high pressure system became established over the Tasman Sea, the north to north-westerly air flow advected heat into S.E. Australia. The heatwave was briefly interrupted by a trough passing through the study region on 18–19th January but quickly returned and intensified from the 22nd January. In this study, we focus on the latter two phases of this heatwave which particularly severely impacted S.E. Australia.

2.2. Model description

To carry out our simulations we used the WRF-LIS-CABLE modelling system. This system includes the CABLE LSM and the National Aeronautics and Space Administration (NASA) Unified Weather Research and Forecasting (NU-WRF) model version 9.2 (v9.2). NU-WRF v9.2 includes the Weather Research and Forecasting Model (WRF) atmospheric model (version 3.9.1) and the Land Information System (LIS) model framework (version 7.2), which is used to couple WRF with CABLE. To force the model, we use the ERA interim data (Berrisford et al., 2011) as boundary conditions for NU-WRF. We follow the WRF atmospheric physics configurations used in Hirsch and King (2020) which includes the New Tiedtke cumulus convection scheme, the WRF Single-Moment 5-class microphysics scheme, the Mellor-Yamada-Janjic boundary layer and surface layer schemes, as well as the RRTMG shortwave and longwave radiation schemes. This version was thoroughly evaluated by Hirsch et al. (2019) with a focus on temperature and rainfall averages and extremes. Their evaluation of this configuration shows good performance in simulating extreme temperatures over S.E. Australia, in particular for the summer season. The model is not perfect of course and tends to simulate too narrow a range of temperature on diurnal scales by underestimating daily maximum temperatures (by up to 4 °C in some regions, their Fig. 4g) and overestimating daily minimum temperatures during heat extremes.

The LSM used in this study is built from CABLE version 2.0, but includes improved hydrological modules described by Decker (2015) and Decker et al. (2017) (hereafter CABLE-GW). These improvements include a groundwater component with unconfined aquifer and sub-grid runoff parameterizations. This version was evaluated by Decker (2015),

Ukkola et al. (2016) and Mu et al. (2021a, 2021b) and demonstrated good performance in simulating land water fluxes during climate extremes. The CABLE-GW was also shown to reproduce observed hydrological data including the Gravity Recovery and Climate Experiment (GRACE) well (Mu et al., 2021b).

2.3. Experimental design

We ran two experiments, one including groundwater (GW) and one assuming free drainage (FD). To obtain the equilibrated initial state for soil moisture, we first use the observation-based Australian Water Availability Project (AWAP) dataset (Jones et al., 2009) to force the CABLE LSM offline for 90 years by repeating the meteorology between 1970 and 1999. This off-line spin-up is designed to create a realistic initial state while remaining computationally feasible. The AWAP dataset used in the simulations has been resampled from daily to 3-hourly temporal resolution via the weather generator developed by Haverd et al. (2013), and re-gridded from 5 km to 10 km resolution. This re-gridding balances the computing cost with the spatial representation of soils and vegetation over S.E. Australia. Following the 90-year spin-up, we then conduct the GW and FD experiments offline from 1970 to 2019 with time varying CO_2 and saving the daily restart file over the last 20 years. These restart files are then used to initialize the coupled WRF-LIS-CABLE model. The overall offline spin-up processes are the same as used by Mu et al. (2021b) but at 10 km resolution and for the whole of Australia.

Following Ge et al. (2019) we initialize WRF-LIS-CABLE for 10, 9, 8, 7 and 6 days before the selected heatwaves (Table 1), and run the model through the heatwave period ending five days after the event, on a domain over S.E. Australia (Fig. 1a) at 25 km. These simulations provide five ensemble members and for each event and each experiment (GW/FD). In the following spatial maps, we display the average of the five ensembles but show the range of the ensembles in time-series figures.

In all simulations, we use observationally-based land surface properties following Mu et al. (2021b). Land cover type is derived from the National Dynamic Land Cover Data of Australia mapped on to CABLE land cover types (see Mu et al. 2021b). The leaf area index (LAI) is prescribed using the Copernicus Global Land Service product (Fuster et al., 2020). Soil parameters are derived from SoilGrids (Hengl et al., 2017) via the pedotransfer functions in Cosby et al. (1984) (note these parameters do not vary with depth).

2.3.1. Groundwater experiment (GW)

The GW experiment uses the default CABLE-GW model which adopts the modified Richards equation (Zeng and Decker, 2009) to solve the vertical water movement among the soil column:

$$\frac{\partial \theta}{\partial t} = -\frac{\partial}{\partial z} K \frac{\partial}{\partial z}(\Psi - \Psi_E) - F \tag{1}$$

where θ ($mm^3\ mm^{-3}$) is the soil volumetric water content, K ($mm\ s^{-1}$) is the parameter of hydraulic conductivity, Ψ (mm) and Ψ_E (mm) are the soil matric potential and the equilibrium soil matric potential, F ($mm\ s^{-1}$) is the sum of subsurface runoff and transpiration, and t (s) and z (mm) are the time and the soil depth dimensions (Decker, 2015). An unconfined groundwater aquifer is implemented as the lower boundary condition to the soil column by solving a simple water balance model:

$$\frac{dW_{aq}}{dt} = q_{re} - q_{aq,sub} \tag{2}$$

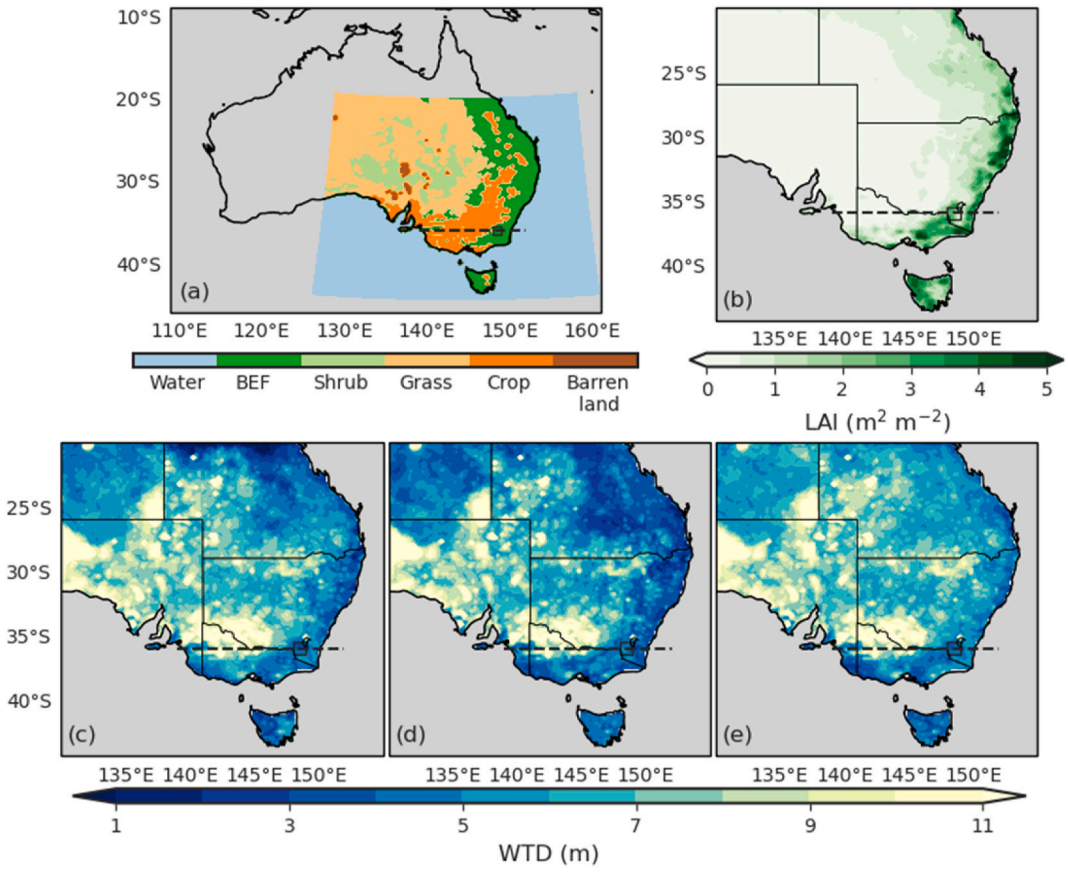

Fig. 1. Land cover type, leaf area index (LAI) and water table depth (WTD) over S.E. Australia. Panel a and b show the model inputs of the land cover types and the January LAI. Panels c–e are the simulated WTD in the 2009, 2013 and 2019 heatwaves. The gray areas in panel a are beyond our simulation domain. The black dash line indicates the transect along 36°S used in Figs. 4–6 and the black box shows the selected shallow WTD region (148-149°E, 35.5–36.5°S) in Fig. 7.

where W_{aq} (mm) is the water mass of the aquifer but in the units of mm, $q_{aq,sub}$ (mm s^{-1}) is the subsurface runoff from the aquifer, and q_{re} (mm s^{-1}) is the water flow between the bottom soil layer and the aquifer. Specifically, a positive q_{re} refers to the groundwater recharge from soil column and a negative q_{re} represents the groundwater discharge to the upper soil column. The q_{re} is computed by the modified Darcy's law:

$$q_{re} = \frac{(K_{aq} + K_{bot})}{2} \frac{(\Psi_{aq} - \Psi_n) - (\Psi_{E,aq} - \Psi_{E,n})}{z_{wtd} - z_n} \quad (3)$$

where K_{aq} (mm s^{-1}) and K_{bot} (mm s^{-1}) are the hydraulic conductivity in the aquifer and the bottom soil layer. Ψ_{aq} (mm) and Ψ_n (mm) are the soil matric potentials for the aquifer and the bottom soil layer, and $\Psi_{E,aq}$ (mm) and $\Psi_{E,n}$ (mm) are the equilibrium soil matric potentials for the aquifer and the bottom soil layer. z_{wtd} (mm) and z_n (mm) are the depth of the water table and the lowest soil layer. A zero flux condition is imposed at the base of the aquifer. The thickness of the aquifer depends on the location of the bedrock and varies spatially. The subsurface runoff (q_{sub}, mm s^{-1}) is topography-dependent and generated from the saturated soil layers and the aquifer:

$$q_{sub} = \sin\frac{\overline{d_z}}{d_l} \widehat{q}_{sub} e^{-\frac{z_{wtd}}{f}} \quad (4)$$

where $\frac{\overline{d_z}}{d_l}$ is the mean subgrid-scale slope, $\widehat{q}_{sub}$ (mm s^{-1}) is the maximum subsurface drainage rate and f is the decay factor originally determined by model calibration against the hydrograph recession curve (Niu et al., 2005).

An important component of CABLE-GW is the soil water stress factor, β, which is defined as:

$$\beta = \sum_{i=1}^{n} f_{root,i} \frac{\theta_i - \theta_{w,i}}{\theta_{fc,i} - \theta_{w,i}} \quad (5)$$

where θ_i (mm^3 mm^{-3}) is the volumetric soil moisture content, $\theta_{fc,i}$ (mm^3 mm^{-3}) is the field capacity, $\theta_{w,i}$ (mm^3 mm^{-3}) is the wilting point, $f_{root,i}$ is the root mass fraction, and i refers to the i th soil layer. β reflects the constraint of soil moisture availability, weighted by the fraction of roots in each layer, on transpiration.

2.3.2. Free drainage experiment (FD)

The FD experiment design follows Mu et al. (2021b) by decoupling the groundwater aquifer from the bottom soil layer. At the interface between the bottom soil layer and the aquifer, soil water can only move downwards as vertical drainage at the rate defined by the bottom soil layer's hydraulic conductivity:

$$q_{re} = K_{bot} \quad (6)$$

This vertical drainage is directly added to the subsurface runoff flux:

$$q_{sub} = q_{sub} + q_{re} \quad (7)$$

In the FD experiment, we assume a fixed water table depth (WTD) at 10 m to remove an artefact caused by the unrealistic WTD estimation associated with the FD implementation.

3. Results

3.1. Groundwater impact on the surface water and energy balance

During heatwave periods, the addition of groundwater access leads to a clear decrease in soil water stress (Equation (5)) by ≤ 70% ($\Delta\beta$, Fig. 2a) in regions of broadleaf evergreen forest (see Fig. 1a) of the

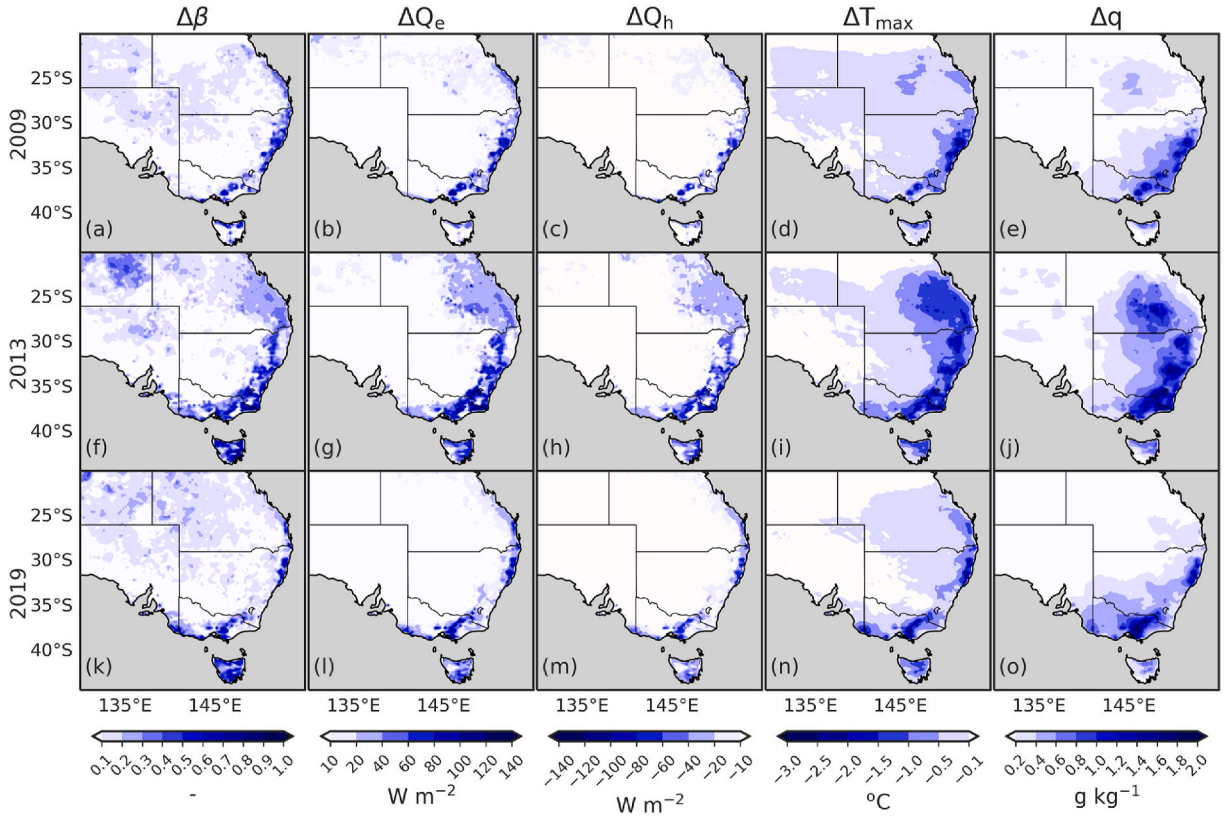

Fig. 2. Simulations of the impact of groundwater on the soil water stress factor ($\Delta\beta$, left column), surface latent heat flux (ΔQ_e, W m^{-2}, middle left), sensible heat flux (ΔQ_h, W m^{-2}, middle), maximum air temperature (ΔT_{max}, °C, middle right), and specific humidity (Δq, g kg^{-1}, right) over S.E. Australia (GW−FD) averaged over the 2009 (top), 2013 (middle) and 2019 (bottom) heatwaves.

eastern and southeastern parts of Australia. The presence of groundwater, particularly shallow WTD (<5 m, Fig. 1c–e), moistens the soil relative to the FD simulation. This greater soil moisture availability results in increased Q_e (Fig. 2b) by up to 120 W m^{-2} relative to FD, largely in those areas with broadleaf evergreen forest and shallow groundwater. Q_h is reduced by up to 100 W m^{-2} (Fig. 2c). The reduction of Q_h is caused by the cooler land surface and due to energy balance constraints with a higher Q_e. There is also an increase in the net radiation at the surface (2–20 W m^{-2}, Fig. 3a) associated with an increase in the net longwave flux (Fig. 3b). The increase in the net longwave flux is caused by a reduction in the upwelling longwave flux (Fig. 3c) with negligible changes in the downwelling longwave (Fig. 3d). Note there are few changes in the solar radiation flux (Fig. 3e). The impacts of GW during heatwaves therefore cools the maximum surface temperature (T_{max}) not only through evaporative cooling, but also to a lesser extent by altering the upwelling longwave radiation. These changes in the surface energy fluxes lead to a reduction in the heatwave intensity by up to 3 °C (Fig. 2d) and an increase in the air humidity by up to 1 g kg^{-1} (Fig. 2e). Thus a cooler and moister atmosphere can result from the existence of shallow groundwater during heatwaves.

The results for all three heatwaves are similar although note the extent of the cooling in T_{max} and its spatial pattern is different across the three events. The impact of adding groundwater is larger in southeastern Queensland in 2013 is smaller in comparison to 2009 or 2019. The differences between these heatwaves are associated with the WTD distributions (Fig. 1c-e). In the 2013 heatwave, the WTD is shallower overall than in 2009 and 2019 owing to both heatwaves in 2009 and 2019 occurring during multi-year droughts, while 2013's heatwave is relatively wet. The impact of groundwater is therefore more significant in the heatwave of 2013 rather than during 2009 or 2019. However, in all three heatwaves, the impact away from forested regions (Fig. 1a) with shallow groundwater is generally small (e.g. cooling of <0.5 °C).

3.2. Groundwater impact on the atmospheric boundary layer

Importantly, the changes in the partitioning of available energy between Q_e and Q_h, and the decrease in the upwelling longwave radiation are large enough to affect the atmosphere (Fig. 4). We next examine a transect at 36°S in the 2013 heatwave as an example (see the black dashed line in Fig. 1). This transect was chosen to include a range of vegetation types and a range of WTDs. The cooling in the maximum potential temperature (θ_{max}) extends to around 2 500 m (>1 °C, Fig. 4a) during the daytime (note this cooling is largely constrained to within the ABL). The reduction in Q_h leads to a decline of daytime ABL height by ~100 m. These changes are largely restricted to the areas of broadleaf evergreen forest with a higher LAI (Fig. 1a and b) and shallow WTD (see blue-yellow insert on each panel) with a negligible impact west of ~147°E where croplands are associated with a deeper WTD (>5m). The impact of groundwater is also larger during the day time associated with higher transpiration. The impact at night on minimum potential temperatures (θ_{min}) is small (<0.5 °C) but is not constrained to the night time ABL. The heat difference above ABL has the potential to contribute to the θ_{max} differences within the ABL during the next day (Miralles et al., 2014). With an increase of Q_e, more water vapour is transported to the atmosphere, and the atmospheric specific humidity increases by ~1 g kg^{-1} during the day (Fig. 4c) with much smaller changes at night (Fig. 4d). The results shown in Fig. 4 are similar to those for 2009 (Fig. 5) and 2019 (Fig. 6). However, since both 2009 and 2019 heatwaves occur during multi-year droughts and the WTDs in the two heatwaves are deeper than in 2013's heatwave (Fig. 1c–e), the impact of groundwater on ABL is more significant in the heatwave of 2013 than in 2009's or 2019's heatwave.

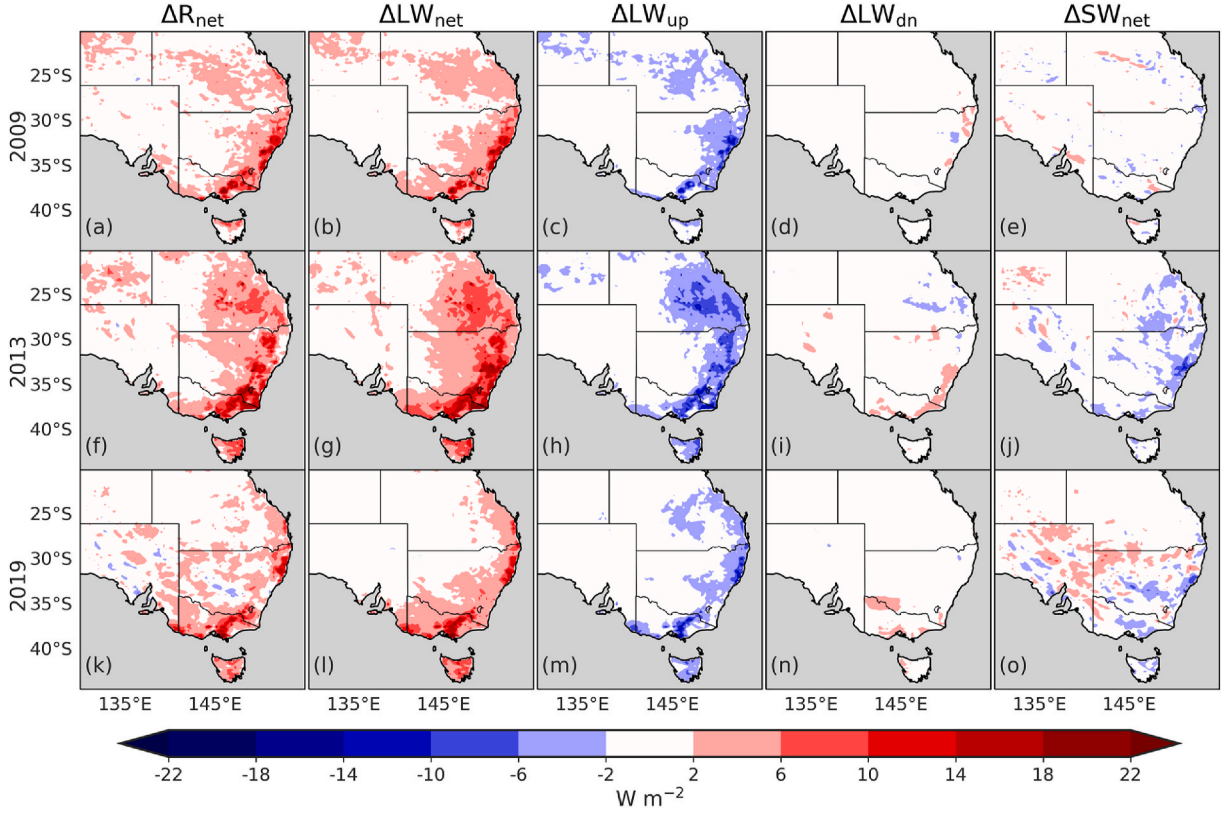

Fig. 3. The impact of groundwater (GW−FD) on net radiation (ΔR_{net}, W m^{-2}, left), net longwave radiation (ΔLW_{net}, W m^{-2}, middle left), upwelling longwave radiation (ΔLW_{up}, W m^{-2}, middle), downwards longwave radiation (ΔLW_{dn}, W m^{-2}, middle right) and net shortwave radiation (ΔSW_{net}, W m^{-2}, right). The top, middle and bottom rows are for 2009, 2013 and 2019 heatwaves respectively. Note that ΔR_{net}, ΔLW_{net} and ΔSW_{net} are calculated at the land surface while ΔLW_{up}, ΔLW_{dn} are calculated at the bottom atmospheric layer.

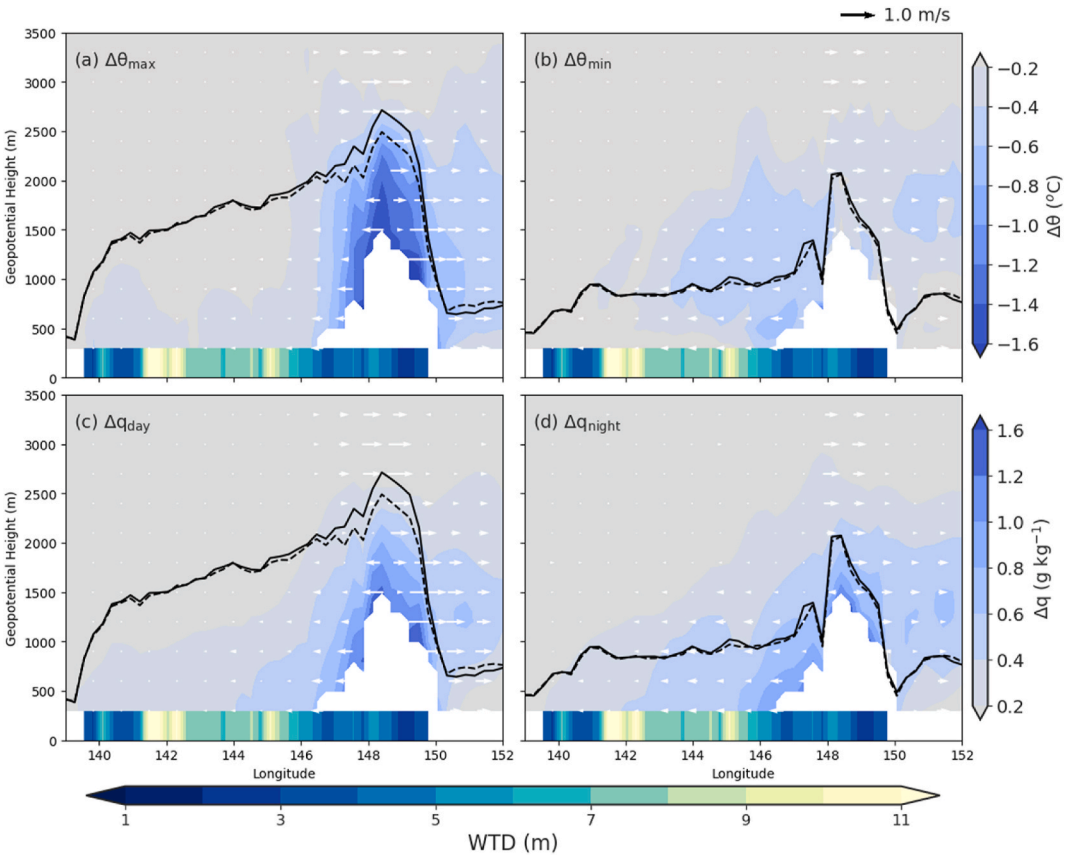

Fig. 4. The impact of groundwater (GW−FD) on the vertical profile of key atmospheric variables along a 36°S transect for the 4–January 18, 2013 heatwave. In panels a–d, the shading indicates the changes in (a) the maximum potential temperature (θ_{max}, °C), (b) the minimum potential temperature (θ_{min}, °C), (c) the daytime specific humidity (q_{day}, g kg^{-1}) and (d) the night time specific humidity (q_{night}, g kg^{-1}); the black lines are the height of atmospheric boundary layer (ABL, m) in the FD (solid) and the GW (dashed) simulations and the white arrows show the wind difference; the bottom blue-yellow bars indicate the water table depth (WTD, m) and the white area shows the orography and the ocean regions. (For interpretation of the references to color in this figure legend, the reader is referred to the Web version of this article.)

To further examine the influence of shallow WTD on the diurnal cycle, we select a representative region (148-149°E, 35.5–36.5°S) along the transect in Figs. 4–6 to analyze the evolution of the 2 m air temperature (Fig. 7a,c,e) and ABL height (Fig. 7b,d,f). We compared both the diurnal cycle response to adding groundwater and to heatwave conditions. Fig. 7a,c,e demonstrates that groundwater reduces the daytime maximum temperature more than the minimum both before and during the heatwaves. However, the inclusion of groundwater does not impact the timing of the maximum or minimum temperature. The differences between the ensemble members (shading) are negligible for the 2013 heatwave, but are noticeable in the 2009 (Figs. 7c) and 2019 (Fig. 7e) heatwaves. For the ABL height, at this location, adding groundwater reduces the simulated height by ~500 m (Fig. 5b,d,f). The differences between the ensemble members are small relative to the impact of groundwater or the simulated differences between pre- and actual heatwave conditions.

3.3. Groundwater impact and vegetation types

To examine how the influence of groundwater varies across different vegetation types we next focus (Fig. 8) on the connection between the simulated WTD and the changes in ΔT_{max} during heatwave days when the observed daily maximum temperature exceeds the 90th percentile of the 1970–2019 climatology on the corresponding day. In regions with broadleaf evergreen forests (BEF, Fig. 8a), the impact of explicitly simulating the groundwater depends on the WTD at point of the onset of the heatwave. In locations with shallow WTD, the vegetation's access to groundwater (which causes a wetter root zone profile, see green dots at bottom left of Fig. 8a) sustains higher evaporation and cooling of the air temperature by up to 5 °C. Where the groundwater is relatively deep (>5m) changes in ΔT_{max} range from +1.5 °C to -3 °C; as the depth to groundwater increases the range in ΔT_{max} decreases and becomes negligible at WTD >10 m. As the simulated WTD becomes deeper, the groundwater becomes decoupled from the root zone soil moisture (mostly <5 m depth) and does not affect transpiration. In contrast to the BEFs, the impact of groundwater on $\Delta\beta$ and ΔT_{max} is less obvious in cropland regions (Fig. 8b), shrubs (Fig. 8c) and grassland (Fig. 8d). In these non-forest regions, the deeper simulated WTD (~7 m in crops, shrubs; and grasses) limits the capacity of the groundwater to buffer the soil moisture state meaning that evaporative cooling during heatwaves is more closely tied to the state of the shallow soil moisture.

4. Discussion and conclusions

We investigated the impact of groundwater on three major heatwaves that impacted S.E. Australia using the coupled WRF-LIS-CABLE modelling system. Explicitly accounting for groundwater in simulations of these heatwaves led to a cooler and wetter land surface, and a cooler and more humid ABL. The surface maximum daily temperatures during these heatwaves were reduced by up to 3 °C (Fig. 2) and by up to 1 °C through the ABL (Fig. 4). Associated with the cooling, a reduction in the ABL height occurred over the shallow WTD areas. The areas of cooling were largely associated with regions of shallow WTD and evergreen broadleaf forests (Figs. 8 and 1).

The inclusion of groundwater moistened the soil which led to a higher Q_e and lower Q_h. These changes are generally comparable with

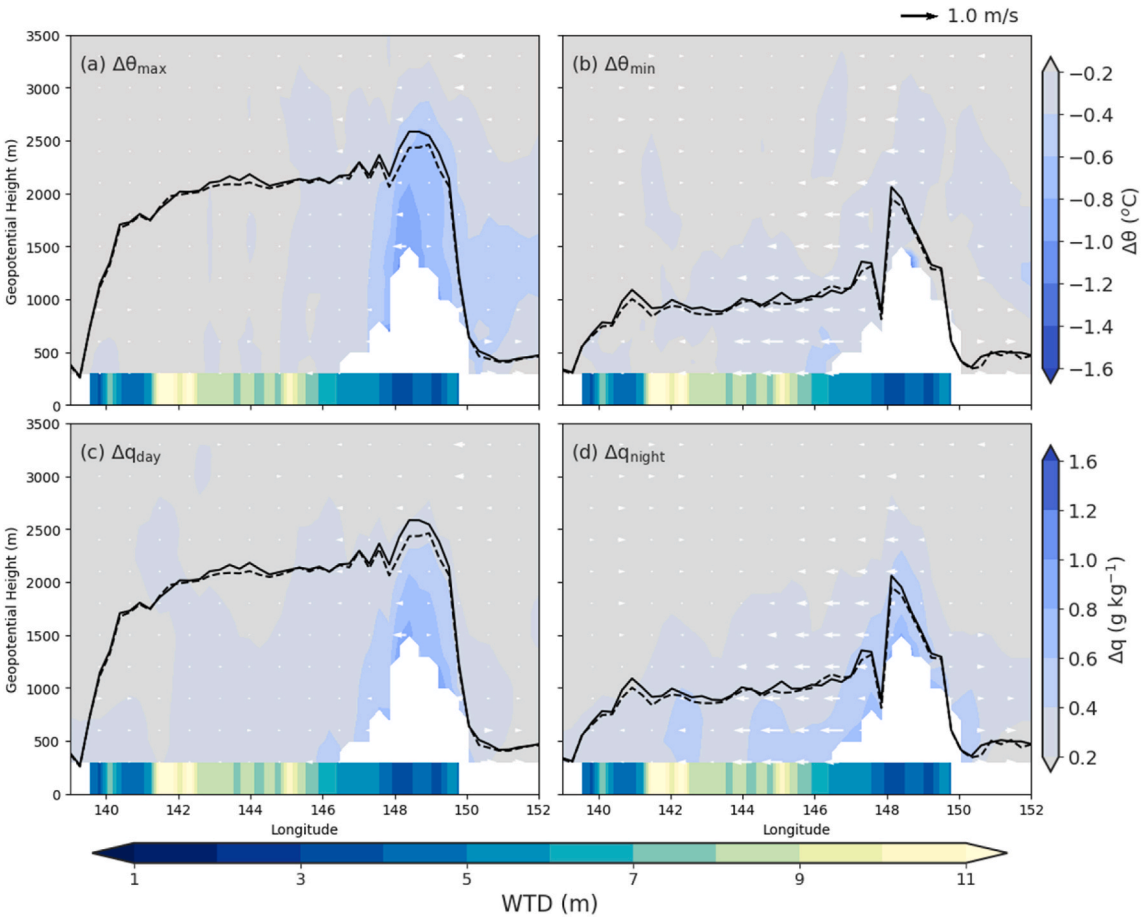

Fig. 5. As Fig. 4, but for the 28 January–February 8, 2009 heatwave.

results from the United States (Anyah et al., 2008; Leung et al., 2011) and Europe (Furusho-Percot et al., 2022; Keune et al., 2016). We note little impact on the simulated precipitation or clouds, a result apparently inconsistent with some earlier researches (Anyah et al., 2008; Jiang et al., 2009; Martinez et al., 2016; Maxwell et al., 2011). However, our simulations focused explicitly on heatwave events which in Australia are associated with blocking high pressure systems, very high temperatures, and a dry and low-cloud atmosphere. We therefore did not find evidence that the increase in Q_e was sufficient to trigger a clear change in rainfall despite a small increase in the specific humidity through the ABL and a slight increase of convective available potential energy (CAPE), which is consistent with the study of 2003 European heatwave in Keune et al. (2016).

Explicitly representing groundwater in a coupled model can therefore moderate the intensity of heatwaves. Three mechanisms influence heatwave intensity. Firstly, groundwater sustains transpiration, which reduces Q_h and the heat transported into the atmosphere. Secondly, as noted by Miralles et al. (2014), heat stored in the ABL can be recycled back to the surface on the next day with an amplification of the heatwave intensity. The lower Q_h in simulations with groundwater reduces the potential for this amplification. Finally, the heat entrained from the free atmosphere is proportional to the time variation of the ABL (Bonetti et al., 2015). Due to the lower Q_h, GW simulations have a lower ABL height during the day but a similar height at night which will tend to lead to less heat being entrained from the free atmosphere into the ABL. These three mechanisms reduce the intensity of our simulated heatwaves by up to 1 °C through the ABL in the shallow WTD regions.

Our analysis of the connections between WTD, soil moisture availability, vegetation type and cooling shows that the soil water stress is the principal constraint on the cooling resulting from the inclusion of groundwater. The presence of a shallow water table increases the root-zone soil moisture availability, leading to higher Q_e (Koirala et al., 2019; Martinez et al., 2016; Maxwell and Kollet, 2008; Mu et al., 2021b; Zipper et al., 2019). However, WTD that leads to a strong response varies between studies (<4 m in Zipper et al., 2019, 1–5 m in Kollet and Maxwell, 2008 or 2–5 m in Leung et al., 2011) depending on the root profile, vegetation characteristics, soil characteristics and how these are implemented in different LSMs. Unfortunately, there are few observations to guide how best to combine all of these elements in LSMs. Despite this uncertainty, basic understanding of terrestrial processes suggests denser vegetation (and/or a higher LAI) will tend to be associated with higher transpiration and greater sensitivity to groundwater depth. This greater sensitivity can be moderated or enhanced depending on the root distribution pointing to the challenges associated with capturing species' dependent root properties, particularly where phreatophytic species exhibit very deep roots (Canadell et al., 1996; Warren et al., 2015).

Another important factor is the plants' sensitivity to high temperatures and the associated vapour pressure gradient (VPD) which can lead to stomatal closure during heatwave extremes. A key area for future work remains to probe whether models accurately capture the thresholds that induce stomatal closure during extremes. Eucalyptus species, common in S.E. Australia, appear to have a greater tolerance of high temperature (including the potential to acclimate; e.g. Aspinwall et al., 2016) and VPD than is typically parameterized in LSMs (Drake et al., 2017; Mu et al., 2021a; Yang et al., 2019). Applications of LSMs in Australian environments may therefore underestimate the potential for evaporative cooling during heatwaves.

We note some limitations in our study. The groundwater module we implement only considers the vertical water movement between the soil and groundwater aquifer and ignores lateral flows between grid cells.

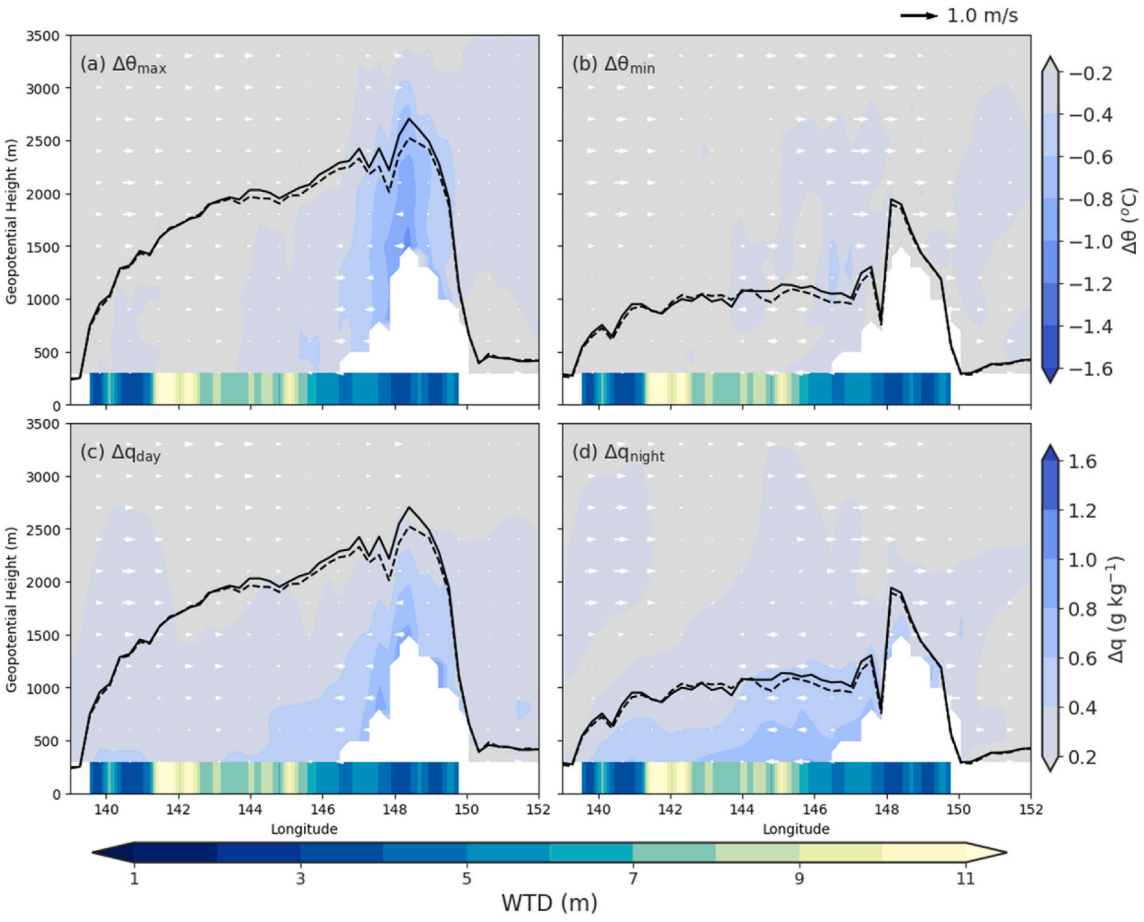

Fig. 6. As Fig. 4, but for the 14–January 26, 2019 heatwave.

Omitting lateral flow means low elevations, where moisture would tend to converge, will tend to simulate a deeper WTD while higher elevations will tend to simulate a shallower WTD than the realistic situations (Barlage et al., 2021; Forrester and Maxwell, 2020; Zeng et al., 2018). However, due to the coarser spatial resolution adopted in our simulations, the impact of topography on WTD distribution via lateral flow is unlikely to significantly affect our conclusions. The root parameterisation we use is relatively simple and may underestimate the role of tree species with deep root water access. We note that our experiments are also dependent to a degree on the choice of the boundary layer, resolution and other physical parameterisation used in WRF. The spatial resolution chosen was a compromise between representing spatial patterns, computational cost and availability of input data for soils and vegetation. Future work that used a higher spatial resolution may lead to regional-scale difference; however, we anticipate the broad conclusions with respect to the influence of groundwater and the link to deep rooted vegetation is robust. In terms of our experimental design, we perform a long uncoupled simulation to reach equilibrium, followed by a further 30 years (1970–1999) to account for the recent climate experienced in this region. Any biases in the simulation of groundwater dynamics, or the coupling with the root zone, will tend to be amplified by this approach due to lack of compensating feedbacks that occur in coupled simulations, with consequences for the simulated WTD. The detailed spatial patterns should therefore be interpreted with care (e.g. Fig. 2) but we are confident that the overall direction of changes simulated are robust (see evaluation against GRACE data in Mu et al., 2021b). The ABL and land surface equilibrate much more quickly than the groundwater and should be robust to this spin-up process.

The surface and ABL cooling induced by shallow groundwater coincident with forests has implications for simulations of heatwave intensity. For weather forecasting, over S.E. Australia, our results suggest the need to include groundwater in spin-up simulations for initial conditions else the soil profile will be too dry and excessively high temperatures will be forecast. The Land Information System enables different timescales of equilibration to be accounted for in creating initial conditions for weather forecasting. For decadal prediction, including groundwater will reduce the risk of extreme temperatures. Climate projections suggest a high risk of worsening heatwaves over S.E. Australian under global warming. Over most regions, groundwater is too deep to influence these simulations, but in regions of shallow WTD, failure to include these processes will lead to an overestimation of the future risk of heatwaves. The influence of shallow groundwater is spatially heterogeneous and influenced by the land cover type and characteristics and we find no evidence that in sparsely vegetated regions, or where the WTD is deep, the omission of groundwater in simulations will introduce systematic errors. Finally, we also note humans are using groundwater unsustainably in some regions (Aeschbach-Hertig and Gleeson, 2012; Bierkens and Wada, 2019; Stokstad, 2020; Wada et al., 2012) and are deforesting regions for agriculture (Curtis et al., 2018). Deforestation, where replaced by more shallow rooted crops, will tend to decouple groundwater from the atmosphere. Similarly, unsustainable use of groundwater will tend to deepen the groundwater and tend to decouple the groundwater from the atmosphere (Barron et al., 2014; Condon and Maxwell, 2019; Keune et al., 2018). In both cases, this has the potential to increases the risk of more intense heatwaves.

We have shown that groundwater has important impacts on the surface and the ABL, in particular where the groundwater is relatively shallow and overlain by forests. It is difficult to speculate in detail on how our results might translate to other regions of the world with different meteorological conditions, different lengths of heatwave,

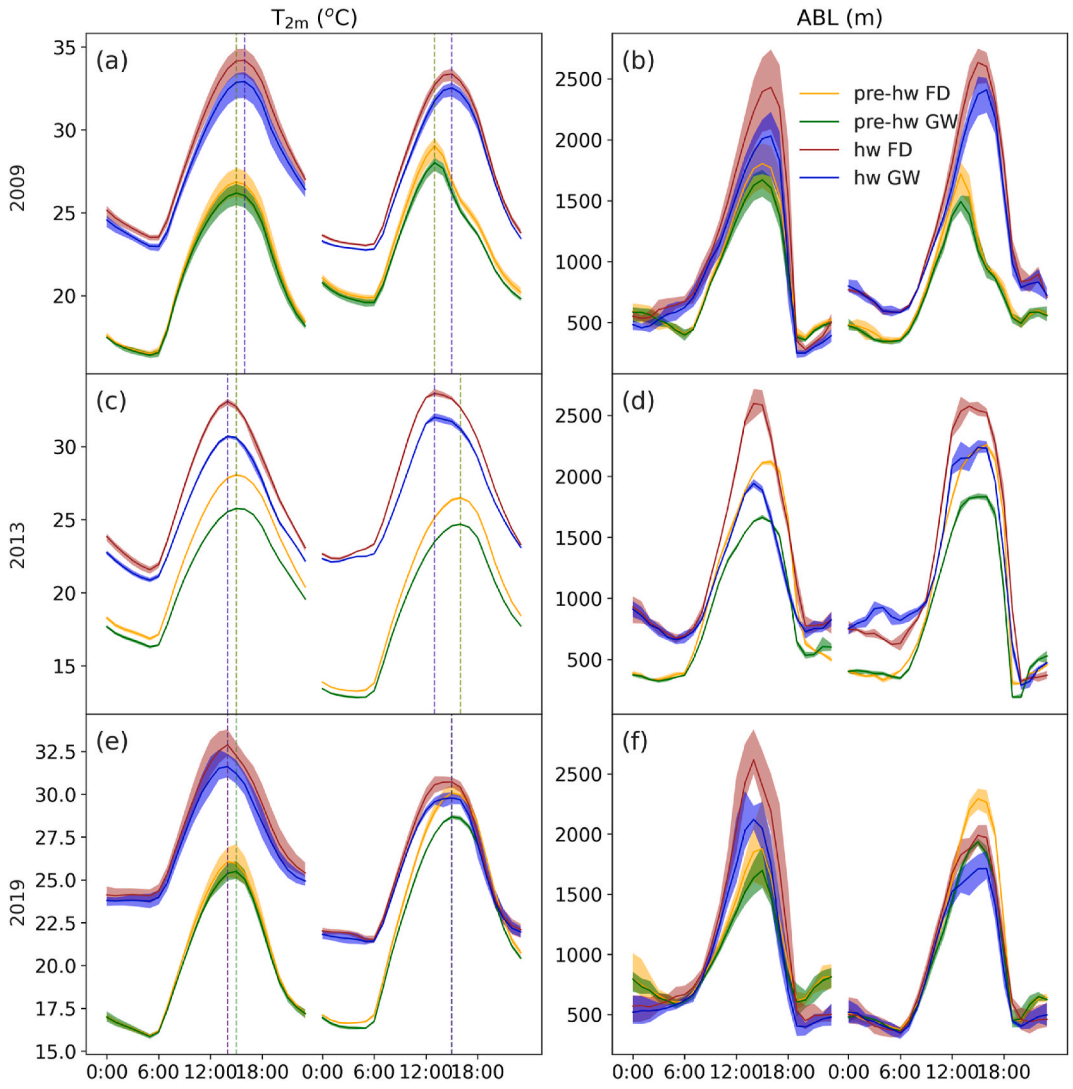

Fig. 7. Diurnal cycle of the 2 m air temperature (T_{2m}, °C, left column) and the ABL height (m, right column) over a shallow WTD region shown by the black box in Fig. 1. Red (FD) and blue (GW) lines refer to the multi-day averaged diurnal cycle in each selected peak phase of the heatwave (hw) event see Table 1. Orange (FD) and green (GW) lines are for the multi-day averaged diurnal cycle before each selected peak phase of the heatwave event (pre-hw). The shadings highlight the uncertainties among ensemble members and the vertical dashed lines in the left column highlights the timing of the temperature maximum. Note that the second peak phase of 2013 heatwave is missed in this figure due to its short interval to the earlier and later peak phases. (For interpretation of the references to color in this figure legend, the reader is referred to the Web version of this article.)

different vegetation types and different hydrological environments. However, the mechanisms we identify are likely to be generic implying there would be value in a more widespread examination of the role of groundwater in influencing land-atmosphere processes. There is, for example, evidence for a strong role of groundwater over North America (Barlage et al., 2021; Ferguson and Maxwell, 2010) and Europe (Furusho-Percot et al., 2022; Keune et al., 2016; Martínez-de la Torre and Miguez-Macho, 2019) in particular where the land was strongly coupled to the atmosphere. Including shallow groundwater in these regions improves the simulations in regional climate models (Barlage et al., 2015; Furusho-Percot et al., 2022). Experiments of the kind we report in regional model intercomparison projects (e.g. https://cordex.org) could therefore be particularly useful. While there are multiple studies focusing on the significance of groundwater on land-atmosphere systems on a seasonal to decadal scales, the examination of the role of groundwater on heatwaves is still rare. We also note that projections of future heatwaves point to more common, and more extreme events. This suggests attention to groundwater, and changes in groundwater, should be a priority for future climate projections over Australia as well as other parts of the world.

Credit author statement

Mengyuan Mu: Conceptualization, Methodology, Software, Formal analysis, Investigation, Writing - Original Draft, Writing - Review & Editing, **Andy Pitman**: Conceptualization, Methodology, Formal analysis, Resources, Supervision, Writing - Original Draft, Writing - Review & Editing, **Martin De Kauwe**: Conceptualization, Formal analysis, Writing - Review & Editing, **Anna Ukkola**: Formal analysis, Writing - Review & Editing, **Jun Ge**: Methodology, Writing - Review & Editing.

Key points

- Shallow groundwater reduces heatwave intensity up to 3 °C, particularly in forested areas
- Groundwater access cools and moistens atmospheric boundary layer during heatwaves

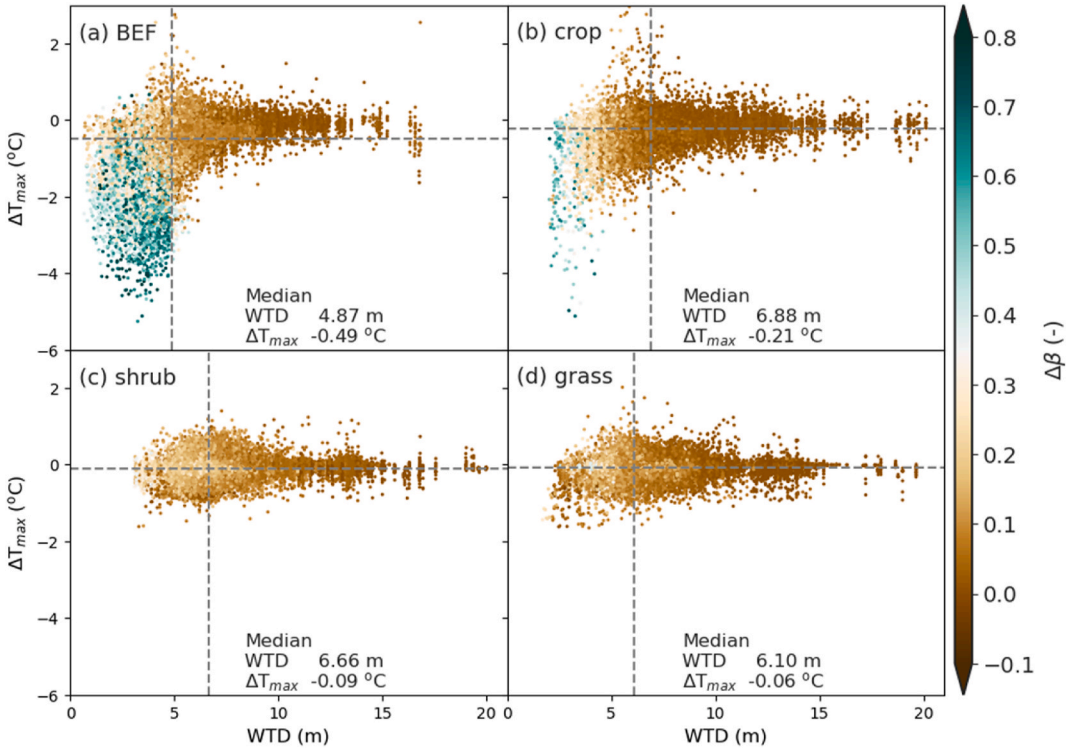

Fig. 8. The dependence (GW−FD) of the impact of groundwater on maximum air temperature (ΔT_{max}) as a function of water table depth (WTD, m) during 2009, 2013 and 2019 heatwave days for (a) broadleaf evergreen forest (BEF), (b) crop, (c) shrub and (d) grass. We use the AWAP observations to calculate the 90th percentile of daily maximum temperature on the corresponding day in 1970–2019 as the threshold to select the heatwave days when the observed daily maximum temperature above the threshold. The color of each dot represents the water stress factor difference ($\Delta\beta$). The vertical and horizontal dashed lines refer to the median of WTD and the median of ΔT_{max} for each vegetation type. (For interpretation of the references to color in this figure legend, the reader is referred to the Web version of this article.)

- Groundwater impacts on atmospheric variables are largely constrained to regions of shallow water table depth

Declaration of competing interest

The authors declare that they have no known competing financial interests or personal relationships that could have appeared to influence the work reported in this paper.

Acknowledgments

The research was funded by the ARC Centre of Excellence for Climate Extremes (CE170100023) and by the New South Wales Department of Planning, Industry and Environment. Mu acknowledges support from the UNSW University International Postgraduate Award (UIPA) scheme, and acknowledges the help from Dr. Annette L. Hirsch and Dr. Claire C. Carouge on NU-WRF set-up. De Kauwe and Pitman acknowledge support from the ARC Discovery Grant (DP190101823) and Ukkola acknowledges support from the ARC Discovery Early Career Researcher Award (DE200100086). De Kauwe acknowledges support from the NSW Research Attraction and Acceleration Program (RAAP). Ge acknowledges the support from the Natural Science Foundation of China (42005096). We are grateful to the National Computational Infrastructure at the Australian National University for provision of supercomputing resources.

References

Aeschbach-Hertig, W., Gleeson, T., 2012. Regional strategies for the accelerating global problem of groundwater depletion. Nat. Geosci. 5 (12), 853–861. https://doi.org/10.1038/ngeo1617.

Anyah, R.O., Weaver, C.P., Miguez-Macho, G., Fan, Y., Robock, A., 2008. Incorporating water table dynamics in climate modeling: 3. Simulated groundwater influence on coupled land-atmosphere variability. J. Geophys. Res. 113 (D7), D07103 https://doi.org/10.1029/2007JD009087.

Aspinwall, M.J., Drake, J.E., Campany, C., Vårhammar, A., Ghannoum, O., Tissue, D.T., Reich, P.B., Tjoelker, M.G., 2016. Convergent acclimation of leaf photosynthesis and respiration to prevailing ambient temperatures under current and warmer climates in Eucalyptus tereticornis. New Phytol. 212 (2), 354–367. https://doi.org/10.1111/nph.14035.

Barlage, M., Chen, F., Rasmussen, R., Zhang, Z., Miguez-Macho, G., 2021. The importance of scale-dependent groundwater processes in land-atmosphere interactions over the Central United States. Geophys. Res. Lett. 48 (5) https://doi.org/10.1029/2020GL092171.

Barlage, M., Tewari, M., Chen, F., Miguez-Macho, G., Yang, Z-L, Niu, G-Y, 2015. The effect of groundwater interaction in North American regional climate simulations with WRF/Noah-MP. Climatic Change 129 (3–4), 485–498. https://doi.org/10.1007/s10584-014-1308-8.

Barron, O., Froend, R., Hodgson, G., Ali, R., Dawes, W., Davies, P., McFarlane, D., 2014. Projected risks to groundwater-dependent terrestrial vegetation caused by changing climate and groundwater abstraction in the Central Perth Basin, Western Australia. Hydrol. Process. 28 (22), 5513–5529. https://doi.org/10.1002/hyp.10014.

Bergstrom, D.M., Wienecke, B.C., Hoff, J., Hughes, L., Lindenmayer, D.B., Ainsworth, T. D., Baker, C.M., Bland, L., Bowman, D.M.J.S.J., Brooks, S.T., Canadell, J.G., Constable, A.J., Dafforn, K.A., Depledge, M.H., Dickson, C.R., Duke, N.C., Helmstedt, K.J., Holz, A., Johnson, C.R., McGeoch, M.A., Melbourne-Thomas, J., Morgain, R., Nicholson, E., Prober, S.M., Raymond, B., Ritchie, E.G., Robinson, S.A., Ruthrof, K.X., Setterfield, S.A., Sgrò, C.M., Stark, J.S., Travers, T., Trebilco, R., Ward, D.F.L., Wardle, G.M., Williams, K.J., Zylstra, P.J., Shaw, J.D., 2021. Combating ecosystem collapse from the tropics to the Antarctic. Global Change Biol. 27 (9), 1692–1703. https://doi.org/10.1111/gcb.15539.

Berrisford, P., Dee, D.P., Poli, P., Brugge, R., Fielding, M., Fuentes, M., Kållberg, P.W., Kobayashi, S., Uppala, S., Simmons, A., 2011. The ERA-Interim Archive Version 2.0, Shinfield Park, Reading [online] Available from: https://www.ecmwf.int/node/8174.

Bierkens, M.F.P.P., Wada, Y., 2019. Non-renewable groundwater use and groundwater depletion: a review. Environ. Res. Lett. 14 (6), 063002 https://doi.org/10.1088/1748-9326/ab1a5f.

Bonetti, S., Manoli, G., Domec, J.C., Putti, M., Marani, M., Katul, G.G., 2015. The influence of water table depth and the free atmospheric state on convective rainfall predisposition. Water Resour. Res. 51 (4), 2283–2297. https://doi.org/10.1002/2014WR016431.

Borchers Arriagada, N., Bowman, D.M.J.S., Palmer, A.J., Johnston, F.H., 2020. Climate change, wildfires, heatwaves and health impacts in Australia. In: Akhtar, R. (Ed.), Extreme Weather Events and Human Health. Springer International Publishing, Cham., pp. 99–116

Bureau of Meteorology, 2019. Special climate statement 68-widespread heatwaves during December 2018 and January 2019 [online] Available from: http://www.bom.gov.au/climate/current/statements/scs68.pdf. (Accessed 18 May 2020).

Bureau of Meteorology, 2013. Special Climate Statement 43-extreme Heat in January 2013 [online] Available from: http://www.bom.gov.au/climate/current/statements/scs43e.pdf.

Bureau of Meteorology, 2020. State of the Climate 2020. Commonwealth Scientific and Industrial Research Organisation (CSIRO).

Canadell, J., Jackson, R.B., Ehleringer, J.B., Mooney, H.A., Sala, O.E., Schulze, E.-D., 1996. Maximum rooting depth of vegetation types at the global scale. Oecologia 108 (4), 583–595. https://doi.org/10.1007/BF00329030.

Climate Centre, National, 2009. The Exceptional January-February 2009 Heatwave in South-Eastern Australia, Bureau of Meteorology, Special Climate Statement 17. Natl. Clim. Cent. (February), 1–11 [online] Available from: http://www.bom.gov.au/climate/current/statements/scs17c.pdf

Coates, L., Haynes, K., O'Brien, J., McAneney, J., de Oliveira, F.D., 2014. Exploring 167 years of vulnerability: an examination of extreme heat events in Australia 1844–2010. Environ. Sci. Pol. 42, 33–44. https://doi.org/10.1016/j.envsci.2014.05.003.

Condon, L.E., Maxwell, R.M., 2019. Simulating the sensitivity of evapotranspiration and streamflow to large-scale groundwater depletion. Sci. Adv. 5 (6), eaav4574. https://doi.org/10.1126/sciadv.aav4574.

Cosby, B.J., Hornberger, G.M., Clapp, R.B., Ginn, T.R., 1984. A statistical exploration of the relationships of soil moisture characteristics to the physical properties of soils. Water Resour. Res. 20 (6), 682–690. https://doi.org/10.1029/WR020i006p00682.

Curtis, P.G., Slay, C.M., Harris, N.L., Tyukavina, A., Hansen, M.C., 2018. Classifying drivers of global forest loss. Science (80-.) 361 (6407), 1108–1111. https://doi.org/10.1126/science.aau3445.

Decker, M., 2015. Development and evaluation of a new soil moisture and runoff parameterization for the CABLE LSM including subgrid-scale processes. J. Adv. Model. Earth Syst. 7 (4), 1788–1809. https://doi.org/10.1002/2013MS000282. Received.

Decker, M., Or, D., Pitman, A., Ukkola, A., 2017. New turbulent resistance parameterization for soil evaporation based on a pore-scale model: impact on surface fluxes in CABLE. J. Adv. Model. Earth Syst. 9 (1), 220–238. https://doi.org/10.1002/2016MS000832.

Doody, T.M., Barron, O.V., Dowsley, K., Emelyanova, I., Fawcett, J., Overton, I.C., Pritchard, J.L., Van Dijk, A.I.J.M., Warren, G., 2017. Continental mapping of groundwater dependent ecosystems: a methodological framework to integrate diverse data and expert opinion. J. Hydrol. Reg. Stud. 10, 61–81. https://doi.org/10.1016/j.ejrh.2017.01.003.

Drake, J.E.E., Power, S.A.A., Duursma, R.A.A., Medlyn, B.E.E., Aspinwall, M.J.J., Choat, B., Creek, D., Eamus, D., Maier, C., Pfautsch, S., Smith, R.A.A., Tjoelker, M.G. G., Tissue, D.T.T., 2017. Stomatal and non-stomatal limitations of photosynthesis for four tree species under drought: a comparison of model formulations. Agric. For. Meteorol. 247 (August), 454–466. https://doi.org/10.1016/j.agrformet.2017.08.026.

Engel, C.B., Lane, T.P., Reeder, M.J., Rezny, M., 2013. The meteorology of black Saturday. Q. J. R. Meteorol. Soc. 139 (672), 585–599. https://doi.org/10.1002/qj.1986.

Evaristo, J., McDonnell, J.J., 2017. Prevalence and magnitude of groundwater use by vegetation: a global stable isotope meta-analysis. Sci. Rep. 7 (March), 44110 https://doi.org/10.1038/srep44110.

Ferguson, I., Maxwell, R., 2010. Role of groundwater in watershed response and land surface feedbacks under climate change. Water Resour. Res. 46 (10), 2009WR008616 https://doi.org/10.1029/2009WR008616.

Forrester, M.M., Maxwell, R.M., 2020. Impact of lateral groundwater flow and subsurface lower boundary conditions on atmospheric boundary layer development over complex terrain. J. Hydrometeorol. 21 (6), 1133–1160. https://doi.org/10.1175/JHM-D-19-0029.1.

Furusho-Percot, C., Goergen, K., Hartick, C., Poshyvailo-Strube, L., Kollet, S., 2022. Groundwater model impacts multiannual simulations of heat waves. Geophys. Res. Lett. 49 (10) https://doi.org/10.1029/2021GL096781.

Fuster, B., Sánchez-Zapero, J., Camacho, F., García-Santos, V., Verger, A., Lacaze, R., Weiss, M., Baret, F., Smets, B., 2020. Quality assessment of PROBA-V LAI, fAPAR and fCOVER collection 300 m products of Copernicus global land Service. Rem. Sens. 12 (6), 1017. https://doi.org/10.3390/rs12061017.

Ge, J., Pitman, A.J., Guo, W., Wang, S., Fu, C., 2019. Do uncertainties in the reconstruction of land cover affect the simulation of air temperature and rainfall in the CORDEX Region of East Asia? J. Geophys. Res.: Atmos. 124 (7), 3647–3670. https://doi.org/10.1029/2018JD029945.

Haverd, V., Raupach, M.R., Briggs, P.R., Canadell, J.G., Isaac, P., Pickett-Heaps, C., Roxburgh, S.H., Van Gorsel, E., Viscarra Rossel, R.A., Wang, Z., 2013. Multiple observation types reduce uncertainty in Australia's terrestrial carbon and water cycles. Biogeosciences 10 (3), 2011–2040. https://doi.org/10.5194/bg-10-2011-2013.

Hengl, T., Mendes de Jesus, J., Heuvelink, G.B.M., Ruiperez Gonzalez, M., Kilibarda, M., Blagotić, A., Shangguan, W., Wright, M.N., Geng, X., Bauer-Marschallinger, B., Guevara, M.A., Vargas, R., MacMillan, R.A., Batjes, N.H., Leenaars, J.G.B., Ribeiro, E., Wheeler, I., Mantel, S., Kempen, B., 2017. SoilGrids250m: global gridded soil information based on machine learning. In: Bond-Lamberty, B. (Ed.), PLoS One 12 (2), e0169748. https://doi.org/10.1371/journal.pone.0169748.

Herold, N., Kala, J., Alexander, L.V., 2016. The influence of soil moisture deficits on Australian heatwaves. Environ. Res. Lett. 11 (6), 064003 https://doi.org/10.1088/1748-9326/11/6/064003.

Hirsch, A.L., King, M.J., 2020. Atmospheric and land surface contributions to heatwaves: an Australian perspective. J. Geophys. Res. Atmos. 125 (17) https://doi.org/10.1029/2020JD033223.

Hirsch, A.L., Kala, J., Pitman, A.J., Carouge, C., Evans, J.P., Haverd, V., Mocko, D., 2014a. Impact of land surface initialization approach on subseasonal forecast skill: a regional analysis in the Southern Hemisphere. J. Hydrometeorol. 15 (1), 300–319. https://doi.org/10.1175/JHM-D-13-05.1.

Hirsch, A.L., Pitman, A.J., Seneviratne, S.I., Evans, J.P., Haverd, V., 2014b. Summertime maximum and minimum temperature coupling asymmetry over Australia determined using WRF. Geophys. Res. Lett. 41 (5), 1546–1552. https://doi.org/10.1002/2013GL059055.

Hirsch, A.L., Kala, J., Carouge, C.C., De Kauwe, M.G., Di Virgilio, G., Ukkola, A.M., Evans, J.P., Abramowitz, G., 2019. Evaluation of the CABLEv2.3.4 land surface model coupled to NU-WRFv3.9.1.1 in simulating temperature and precipitation means and extremes over CORDEX AustralAsia within a WRF physics ensemble. J. Adv. Model. Earth Syst. 11 (12), 4466–4488. https://doi.org/10.1029/2019MS001845.

Jiang, X., Niu, G.-Y., Yang, Z.-L., 2009. Impacts of vegetation and groundwater dynamics on warm season precipitation over the Central United States. J. Geophys. Res. 114 (D6), D06109 https://doi.org/10.1029/2008JD010756.

Jones, D.A., Wang, W., Fawcett, R., 2009. High-quality spatial climate data-sets for Australia. Aust. Meteorol. Oceanogr. J. 58 (04), 233–248. https://doi.org/10.22499/2.5804.003.

Jyoteeshkumar reddy, P., Perkins-Kirkpatrick, S.E., Sharples, J.J., Perkins-Kirkpatrick, S. E., Sharples, J.J., 2021. Intensifying Australian heatwave trends and their sensitivity to observational data. Earth's Future 9 (4), 1–18. https://doi.org/10.1029/2020EF001924.

Kala, J., Andrys, J., Lyons, T.J., Foster, I.J., Evans, B.J., 2015b. Sensitivity of WRF to driving data and physics options on a seasonal time-scale for the southwest of Western Australia. Clim. Dynam. 44 (3–4), 633–659. https://doi.org/10.1007/s00382-014-2160-2.

Kala, J., Evans, J.P., Pitman, A.J., 2015a. Influence of antecedent soil moisture conditions on the synoptic meteorology of the Black Saturday bushfire event in southeast Australia. Q. J. R. Meteorol. Soc. 141 (693), 3118–3129. https://doi.org/10.1002/qj.2596.

Keune, J., Sulis, M., Kollet, S., Siebert, S., Wada, Y., 2018. Human water use impacts on the strength of the continental sink for atmospheric water. Geophys. Res. Lett. 45 (9), 4068–4076. https://doi.org/10.1029/2018GL077621.

Keune, J., Gasper, F., Goergen, K., Hense, A., Shrestha, P., Sulis, M., Kollet, S., 2016. Studying the influence of groundwater representations on land surface-atmosphere feedbacks during the European heat wave in 2003, 13 J. Geophys. Res. Atmos. 121 (22), 301–313. https://doi.org/10.1002/2016JD025426, 325.

Kiem, A.S., Verdon-Kidd, D.C., Boulter, S.L., Palutikof, J.P., 2010. Learning from experience: historical case studies and climate change adaptation. In: Kiem, A.S. (Ed.), National Climate Change Adaptation Research Facility. Gold Coast, Qld.

Koirala, S., Kim, H., Hirabayashi, Y., Kanae, S., Oki, T., 2019. Sensitivity of global hydrological simulations to groundwater capillary flux parameterizations. Water Resour. Res. 55 (1), 402–425. https://doi.org/10.1029/2018WR023434.

Kollet, S.J., Maxwell, R.M., 2008. Capturing the influence of groundwater dynamics on land surface processes using an integrated, distributed watershed model. Water Resour. Res. 44 (2), 1–18. https://doi.org/10.1029/2007WR006004.

Kornhuber, K., Coumou, D., Vogel, E., Lesk, C., Donges, J.F., Lehmann, J., Horton, R.M., 2020. Amplified Rossby waves enhance risk of concurrent heatwaves in major breadbasket regions. Nat. Clim. Change 10 (1), 48–53. https://doi.org/10.1038/s41558-019-0637-z.

Leung, L.R., Huang, M., Qian, Y., Liang, X., 2011. Climate–soil–vegetation control on groundwater table dynamics and its feedbacks in a climate model. Clim. Dynam. 36 (1–2), 57–81. https://doi.org/10.1007/s00382-010-0746-x.

Lewis, S.C., King, A.D., Mitchell, D.M., 2017. Australia's unprecedented future temperature extremes under Paris limits to warming. Geophys. Res. Lett. 44 (19), 9947–9956. https://doi.org/10.1002/2017GL074612.

Luo, X., Liang, X., Lin, J., 2016. Plant transpiration and groundwater dynamics in water-limited climates: impacts of hydraulic redistribution. Water Resour. Res. 52 (6), 4416–4437. https://doi.org/10.1002/2015WR017316.

Martinez, J.A., Dominguez, F., Miguez-Macho, G., 2016. Impacts of a groundwater scheme on hydroclimatological conditions over southern South America. J. Hydrometeorol. 17 (11), 2959–2978. https://doi.org/10.1175/JHM-D-16-0052.1.

Martínez-de la Torre, A., Miguez-Macho, G., 2019. Groundwater influence on soil moisture memory and land–atmosphere fluxes in the Iberian Peninsula. Hydrol. Earth Syst. Sci. 23 (12), 4909–4932. https://doi.org/10.5194/hess-23-4909-2019.

Maxwell, R.M., Kollet, S.J., 2008. Interdependence of groundwater dynamics and land-energy feedbacks under climate change. Nat. Geosci. 1 (10), 665–669. https://doi.org/10.1038/ngeo315.

Maxwell, R.M., Lundquist, J.K., Mirocha, J.D., Smith, S.G., Woodward, C.S., Tompson, A. F.B., 2011. Development of a coupled groundwater–atmosphere model. Mon. Weather Rev. 139 (1), 96–116. https://doi.org/10.1175/2010MWR3392.1.

Merrifield, A.L., Simpson, I.R., McKinnon, K.A., Sippel, S., Xie, S.-P.P., Deser, C., 2019. Local and nonlocal land surface influence in European heatwave initial condition ensembles. Geophys. Res. Lett. 46 (23), 14082–14092. https://doi.org/10.1029/2019GL083945.

Miguez-Macho, G., Fan, Y., Weaver, C.P., Walko, R., Robock, A., 2007. Incorporating water table dynamics in climate modeling: 2. Formulation, validation, and soil

moisture simulation. J. Geophys. Res. Atmos. 112 (D13) https://doi.org/10.1029/2006JD008112, 2006JD008112.
Miralles, D.G., Teuling, A.J., van Heerwaarden, C.C., De Arellano, J.V.G., Vilà-Guerau de Arellano, J., De Arellano, J.V.G., Vilà-Guerau de Arellano, J., 2014. Mega-heatwave temperatures due to combined soil desiccation and atmospheric heat accumulation. Nat. Geosci. 7 (5), 345–349. https://doi.org/10.1038/ngeo2141.
Miralles, D.G., Gentine, P., Seneviratne, S.I., Teuling, A.J., 2019. Land-atmospheric feedbacks during droughts and heatwaves: state of the science and current challenges. Ann. N. Y. Acad. Sci. 1436 (1), 19–35. https://doi.org/10.1111/nyas.13912.
Mu, M., De Kauwe, M.G., Ukkola, A.M., Pitman, A.J., Gimeno, T.E., Medlyn, B.E., Or, D., Yang, J., Ellsworth, D.S., 2021a. Evaluating a land surface model at a water-limited site: implications for land surface contributions to droughts and heatwaves. Hydrol. Earth Syst. Sci. 25 (1), 447–471. https://doi.org/10.5194/hess-25-447-2021.
Mu, M., De Kauwe, M.G., Ukkola, A.M., Pitman, A.J., Guo, W., Hobeichi, S., Briggs, P.R., 2021b. Exploring how groundwater buffers the influence of heatwaves on vegetation function during multi-year droughts. Earth Syst. Dyn. 12 (3), 919–938. https://doi.org/10.5194/esd-12-919-2021.
Niu, G.-Y., Yang, Z.-L., Dickinson, R.E., Gulden, L.E., 2005. A simple TOPMODEL-based runoff parameterization (SIMTOP) for use in global climate models. J. Geophys. Res. 110 (D21), D21106 https://doi.org/10.1029/2005JD006111.
Parker, T.J., Berry, G.J., Reeder, M.J., 2014. The structure and evolution of heat waves in southeastern Australia. J. Clim. 27 (15), 5768–5785. https://doi.org/10.1175/JCLI-D-13-00740.1.
Perkins-Kirkpatrick, S.E., Gibson, P.B., 2017. Changes in regional heatwave characteristics as a function of increasing global temperature. Sci. Rep. 7 (1), 1–12. https://doi.org/10.1038/s41598-017-12520-2.
Perkins-Kirkpatrick, S.E., Lewis, S.C., 2020. Increasing trends in regional heatwaves. Nat. Commun. 11 (1), 3357. https://doi.org/10.1038/s41467-020-16970-7.
Pezza, A.B., van Rensch, P., Cai, W., 2012. Severe heat waves in Southern Australia: synoptic climatology and large scale connections. Clim. Dynam. 38 (1–2), 209–224. https://doi.org/10.1007/s00382-011-1016-2.
Purich, A., Cowan, T., Cai, W., van Rensch, P., Uotila, P., Pezza, A., Boschat, G., Perkins, S., 2014. Atmospheric and oceanic conditions associated with Southern Australian heat waves: a CMIP5 analysis. J. Clim. 27 (20), 7807–7829. https://doi.org/10.1175/JCLI-D-14-00098.1.
Ruthrof, K.X., Breshears, D.D., Fontaine, J.B., Froend, R.H., Matusick, G., Kala, J., Miller, B.P., Mitchell, P.J., Wilson, S.K., van Keulen, M., Enright, N.J., Law, D.J., Wernberg, T., Hardy, G.E.S.J., 2018. Subcontinental heat wave triggers terrestrial and marine, multi-taxa responses. Sci. Rep. 8 (1), 1–9. https://doi.org/10.1038/s41598-018-31236-5.
Stokstad, E., 2020. Deep deficit. Science (80-.) 368 (6488), 230–233. https://doi.org/10.1126/science.368.6488.230.
Teague, B., Pascoe, S., McLeod, R., 2010. The 2009 Victorian Bushfires Royal Commission http://doi.org/APO-22187.
Trancoso, R., Syktus, J., Toombs, N., Ahrens, D., Wong, K.K.-H.H., Pozza, R.D., 2020. Heatwaves intensification in Australia: a consistent trajectory across past, present and future. Sci. Total Environ. 742, 140521 https://doi.org/10.1016/j.scitotenv.2020.140521.
Ukkola, A.M., Pitman, A.J., Decker, M., De Kauwe, M.G., Abramowitz, G., Kala, J., Wang, Y.-P.P., 2016. Modelling evapotranspiration during precipitation deficits: identifying critical processes in a land surface model. Hydrol. Earth Syst. Sci. 20 (6), 2403–2419. https://doi.org/10.5194/hess-20-2403-2016.
Wada, Y., van Beek, L.P.H.H., Bierkens, M.F.P.P., 2012. Nonsustainable groundwater sustaining irrigation: a global assessment. Water Resour. Res. 48 (6) https://doi.org/10.1029/2011WR010562.
Warren, J.M., Hanson, P.J., Iversen, C.M., Kumar, J., Walker, A.P., Wullschleger, S.D., 2015. Root structural and functional dynamics in terrestrial biosphere models – evaluation and recommendations. New Phytol. 205 (1), 59–78. https://doi.org/10.1111/nph.13034.
Wehrli, K., Guillod, B.P., Hauser, M., Leclair, M., Seneviratne, S.I., 2019. Identifying key driving processes of major recent heat waves. J. Geophys. Res. Atmos. 124 (22), 11746–11765. https://doi.org/10.1029/2019JD030635.
Yang, J., Duursma, R.A., De Kauwe, M.G., Kumarathunge, D., Jiang, M., Mahmud, K., Gimeno, T.E., Crous, K.Y., Ellsworth, D.S., Peters, J., Choat, B., Eamus, D., Medlyn, B.E., 2019. Incorporating non-stomatal limitation improves the performance of leaf and canopy models at high vapour pressure deficit. Tree Physiol. 39 (12), 1961–1974. https://doi.org/10.1093/treephys/tpz103.
Zander, K.K., Botzen, W.J.W.W., Oppermann, E., Kjellstrom, T., Garnett, S.T., 2015. Heat stress causes substantial labour productivity loss in Australia. Nat. Clim. Change 5 (7), 647–651. https://doi.org/10.1038/nclimate2623.
Zeng, X., Decker, M., 2009. Improving the numerical solution of soil moisture–based Richards equation for land models with a deep or shallow water table. J. Hydrometeorol. 10 (1), 308–319. https://doi.org/10.1175/2008JHM1011.1.
Zeng, Y., Xie, Z., Liu, S., Xie, J., Jia, B., Qin, P., Gao, J., 2018. Global land surface modeling including lateral groundwater flow. J. Adv. Model. Earth Syst. 10 (8), 1882–1900. https://doi.org/10.1029/2018MS001304.
Zipper, S.C., Keune, J., Kollet, S.J., 2019. Land use change impacts on European heat and drought: remote land-atmosphere feedbacks mitigated locally by shallow groundwater. Environ. Res. Lett. 14 (4), 044012 https://doi.org/10.1088/1748-9326/ab0db3.